Second International Conference on CFD in the Minerals and Process Industries
CSIRO, Melbourne, Australia
6-8 December 1999

DYNAMICS OF SURFACTANT-INFLUENCED GAS/LIQUID INTERFACES

J.M. LOPEZ[1] and A. HIRSA[2]

[1]Dept. of Mathematics, Arizona State University, Tempe, AZ 85287-1804, USA
[2]Dept. of Mech., Aero. Eng. and Mechanics, Rensselaer Polytechnic Institute, Troy, NY 12180-3590, USA
(lopez@math.la.asu.edu, hirsaa@rpi.edu)

ABSTRACT

The presence of surfactants, ubiquitous at most gas/liquid interfaces and particularly at the air/water interface, has a pronounced effect on the stress balance at the interface, and this in turn is nonlinearly coupled to the bulk flow. Forces acting on the interface include surface tension gradients and the viscous resistance to shear and dilation. These viscoelastic properties vary with the surfactant concentration at the interface. The surface tension and surface shear viscosity were measured directly over a range of surface concentration of hemicyanine (an insoluble surfactant). Here, we present a fundamental description of the interface and its coupling to the bulk flow, and develop a Navier-Stokes numerical model. Numerical studies of a canonical flow are presented, comparing contaminated interface cases with that of a clean interface and a rigid no-slip surface, providing added insight into the altered dynamics that result from the presence of a small amount of surfactants.

NOMENCLATURE

c	dimensionless surfactant concentration
c_c	characteristic surfactant concentration
c_o	initial dimensionless surfactant concentration
Ca	capillary number
d	depth of fluid
D_s	surface diffusivity
nr	number of radial nodes
nz	number of vertical nodes
r	dimensionless radial coordinate
r_i	inner cylinder radius
r_o	outer cylinder radius
Re	Reynolds number
Pe^s	surface Peclet number
t	dimensionless time
u	dimensionless radial velocity
v	dimensionless azimuthal velocity
x	dimensionless radial gap coordinate
z	dimensionless axial coordinate
α	dimensionless parameter in (4)
β	dimensionless parameter in (4)
Γ	dimensionless angular momentum
δt	dimensionless time-step
η	dimensionless azimuthal vorticity
κ	dimensionless surface dilatational viscosity
λ	dimensionless surface shear viscosity
μ	dynamic viscosity
μ^s	surface shear viscosity
ν	kinematic viscosity
ρ	density
σ	dimensionless surface tension
σ_c	characteristic surface tension
θ	angular displacement
ψ	dimensionless streamfunction
Ω	angular velocity of the floor

INTRODUCTION

In slightly contaminated situations, particularly when the inertial time scales are small compared to the time scales associated with transport kinetics, the liquid/gas interface tends to be swept clean by the bulk flow in the upstream region, and the surfactant molecules tend to accumulate downstream. The separation between clean and surfactant laden interface tends to be a sharp front. This is readily observed upstream of a surface barrier or on rising bubbles. The location of the front and the concentration level downstream of the front play a major role in determining the dynamics, not only of the flow at the interface, but of the entire coupled interface/bulk flow field. The question naturally arises: What determines the location of the contamination front and the surfactant concentration distribution downstream of it? The answer lies in the coupling between the bulk flow, the Marangoni elasticity, and surface viscous and diffusion effects. The Marangoni elasticity, due to surface tension gradients, and the surface viscosities, are functions of the thermodynamic state of the interface and hence the local concentration. In order to answer the question, one needs to solve a coupled system, consisting of the Navier-Stokes equations for the bulk flow, advection-diffusion of the (active scalar) concentration of surfactant, and the tangential stress balances at the interface. If the interface is not flat, the normal stress balance also needs to be included.

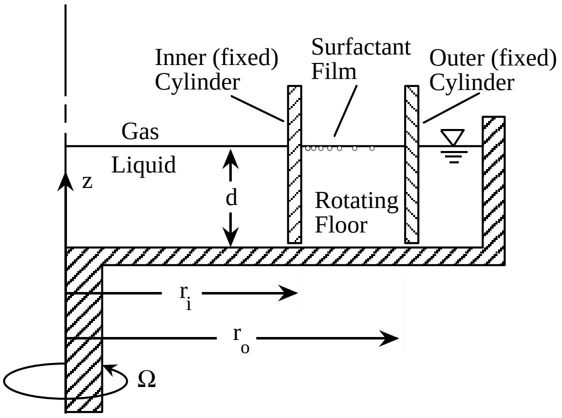

Figure 1: Schematic of the deep-channel viscometer.

GOVERNING EQUATIONS

The flow consists of fluid of density ρ, molecular viscosity μ, and kinematic viscosity ν (the actual experiments use water at room temperature, 23 ± 1 °C), contained in a circular annular region of inner radius r_i and outer radius r_o, filled to a depth d. The two cylinder sidewalls are stationary, and the bottom endwall rotates at a constant rate Ω. The top surface of the fluid is exposed to air, and has a (monomolecular) surfactant film on the interface. Initially, everything is at rest, and a known amount of surfactant is uniformly spread on the interface. At time $t = 0$, the bottom endwall is impulsively started. A schematic of the flow apparatus
is shown in Fig. 1.

The governing equations are the axisymmetric Navier-Stokes equations, together with the continuity equation and appropriate boundary and initial conditions. Using a cylindrical polar coordinate system (r, θ, z) and the Stokes streamfunction ψ, the nondimensional velocity and vorticity vectors are, respectively,

$$\left(-\frac{1}{r}\frac{\partial\psi}{\partial z},\frac{\Gamma}{r},\frac{1}{r}\frac{\partial\psi}{\partial r}\right) \text{ and } \left(-\frac{1}{r}\frac{\partial\Gamma}{\partial z},\eta,\frac{1}{r}\frac{\partial\Gamma}{\partial r}\right).$$

We shall use r_o as the length scale and $1/\Omega$ as the time scale, and define a Reynolds number $Re = \Omega\ r_o^2/\nu$.

The nondimensional axisymmetric Navier-Stokes equations are:

$$\frac{D\Gamma}{Dt} = \frac{1}{Re}\nabla_*^2\Gamma, \tag{1}$$

$$\frac{D\eta}{Dt} + \frac{\eta}{r^2}\frac{\partial\psi}{\partial z} - \frac{1}{r^3}\frac{\partial\Gamma^2}{\partial z} = \frac{1}{Re}\left(\nabla^2\eta - \frac{\eta}{r^2}\right), \tag{2}$$

where

$$\nabla_*^2\psi = -r\ \eta, \tag{3}$$

$$\frac{D}{Dt} = \frac{\partial}{\partial t} - \frac{1}{r}\frac{\partial\psi}{\partial z}\frac{\partial}{\partial r} + \frac{1}{r}\frac{\partial\psi}{\partial r}\frac{\partial}{\partial z},$$

$$\nabla^2 = \frac{\partial^2}{\partial z^2} + \frac{\partial^2}{\partial r^2} + \frac{1}{r}\frac{\partial}{\partial r},$$

$$\nabla_*^2 = \frac{\partial^2}{\partial z^2} + \frac{\partial^2}{\partial r^2} - \frac{1}{r}\frac{\partial}{\partial r}.$$

The boundary conditions on the solid boundaries are no-slip; i.e. the normal and tangential derivatives of ψ vanish, $\Gamma = 0$ on the stationary cylinder walls and $\Gamma = r^2$ on the rotating endwall. The azimuthal vorticity η on the solid boundaries is determined by evaluating (3) on the boundaries once ψ is known. On the air/water interface, being a material surface, ψ is continuous with its value on the sidewalls, which we set to zero without loss of generality. We shall assume that the interface is flat, and hence the contact angle at the air/water/solid is 90° (in the experiments we fix the location of the contact line by depositing a non-wetting parafin film above $z = d$ on the glass walls). This leaves the conditions for Γ and η on the interface to be specified.

Our treatment of the interface follows that of Scriven (1960); except that we allow the surface viscosities to vary with variations in the surfactant concentration (see Lopez & Hirsa, 1998 and Lopez & Chen, 1998) for a detailed treatment). We also allow for a nonlinear equation of state. For hemicyanine at an air/water interface at room temperature, we have measured using standard techniques (Wilhelmy plate measurement with an electrobalance on a Langmuir trough) the surface tension as a function of surfactant concentration, up to a surface coverage where the monolayer undergoes a phase transition (Adamson, 1990 and Gaines, 1966).

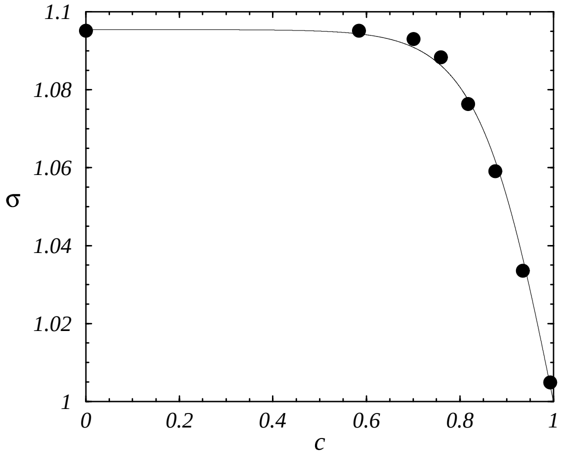

Figure 2: Equation of state, σ vs. c, for hemicyanine at the air/water interface at room temperature; the • symbols are experimental measurements of Hirsa *et al.* (1997), and the solid line is the model eq. (4).

The measured equation of state is presented in Fig. 2, along with a model that fits the data over a large range of c, given by the equation

$$\sigma = 1 + \frac{\alpha}{\sigma_c}\tanh(\beta(1-c)), \tag{4}$$

where the surface tension, σ, has been nondimensionalized with a characteristic surface tension, σ_c = 66 dynes/cm (milli-Newton/m), and the surfactant concentration, c, has been nondimensionalized with the corresponding characteristic concentration, c_c = 0.856 mg/m^2. The two parameters α and β used to match the model to the data are related to the saturation surface pressure, i.e. the range in surface tension between that of a clean interface and a saturated one, and the Marangoni number which is related to the slope of the equation of state at the inflection point. For this particular system, α = 6.3 and β = 6.2. Note that this equation of state is much flatter at small c than the often used Szyskowsky equation (e.g. see Edwards *et al.* 1991) for idealized gas-like surfactants at low concentration. The flat behavior of σ at small c is representative of insoluble monolayers (Gains 1966).

The surface viscosities are also nonlinear functions of the thermodynamic state of the interface. Using a deep channel viscometer, we have measured the surface shear viscosity, μ^s, for our surfactant system over the same range of c as given in the equation of state, and fitted a model equation to the data (see Fig. 3). The model equation for the nondimensional surface shear viscosity is

$$\lambda = 1.15\ \text{x}\ 10^{-3}[-1 + \exp(2.6c)], \tag{5}$$

where $\lambda = \mu^s/(\mu r_o)$. The surface dilatational viscosity, κ (nondimensional), will have to be modeled since it has not yet been measured consistently with any two different experimental techniques for any surfactant (Edwards *et al.* 1991). We shall model κ as being equal to the shear viscosity, $k = \lambda$.

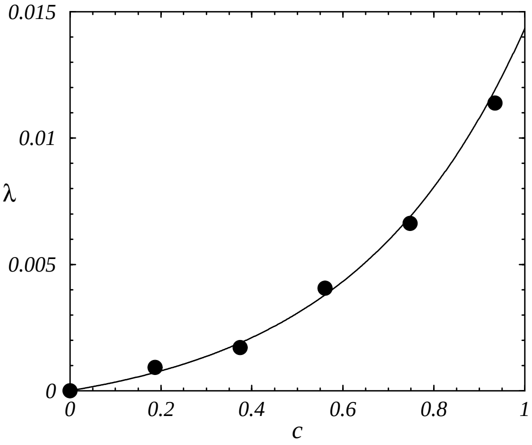

Figure 3: Surface shear viscosity, μ^s vs. c, for hemicyanine at the air/water interface at room temperature; the • symbols are experimental measurements and the solid line is the model eq. (5).

Since the surface tension, σ, and the surface viscosities, λ and κ, are all functions of the surfactant concentration c, we need to solve an active scalar advection-diffusion equation for c:

$$\frac{\partial c}{\partial t} = -\frac{1}{r}\frac{\partial}{\partial r}\left(c\frac{\partial \psi}{\partial z}\right) + \frac{1}{Pe^s}\left(\frac{\partial^2 c}{\partial r^2} + \frac{1}{r}\frac{\partial c}{\partial r}\right), \qquad (6)$$

where $Pe^s = \Omega r_o^2 / D_s$ is the surface Peclet number and D_s is the surface diffusion of the surfactant; D_s is estimated to be of order 10^{-5} cm^2/s for typical surfactants (Agrawal & Neuman 1988). For hemicyanine, Hirsa *et al.* (1997) estimated an upper bound $D_s < 10^{-6}$ cm^2/s. For $Re = 2000$, $\Omega r_o^2 = 20$ cm^2/s ($r_o = 9.61$ cm), and in the computations we use Pe^s up to 10^5; this upper value is essentially determined by the available grid resolution.

For a flat interface, only the tangential stress balance plays a dynamic role. The stress balance in the azimuthal direction is

$$\frac{\partial \Gamma}{\partial z} = \lambda\left(\frac{\partial^2 \Gamma}{\partial r^2} - \frac{1}{r}\frac{\partial \Gamma}{\partial r}\right) + \frac{\partial \lambda}{\partial r}\left(\frac{\partial \Gamma}{\partial r} - \frac{2\Gamma}{r}\right), \qquad (7)$$

and in the radial direction

$$\begin{aligned}\eta = \frac{1}{Ca}\frac{\partial \sigma}{\partial r} + (\lambda + \kappa)\left(\frac{1}{r^2}\frac{\partial^2 \psi}{\partial r \partial z} - \frac{1}{r}\frac{\partial^3 \psi}{\partial r^2 \partial z}\right) - \\ \frac{1}{r}\frac{\partial^2 \psi}{\partial r \partial z}\frac{\partial(\lambda + \kappa)}{\partial r} + \frac{2}{r^2}\frac{\partial \psi}{\partial z}\frac{\partial \lambda}{\partial r},\end{aligned} \qquad (8)$$

where $Ca = \mu \Omega r_o / \sigma_c$ is the capillary number. Both (7) and (8) are solved at the interface $z = d$. The flat interface assumption here is expected to be valid given that the experimental conditions give Froude No. << 1.

NUMERICAL TECHNIQUE

Due to the nonlinear coupling between the bulk flow and the boundary conditions, an explicit time integration is implemented. We begin by discretizing in space using second-order centered differences. Equations (1, 2) then have the form

$$\frac{d\Gamma_{i,j}}{dt} = RHS_1(\Gamma, \psi), \qquad (9)$$

$$\frac{d\eta_{i,j}}{dt} = RHS_2(\eta, \Gamma, \psi). \qquad (10)$$

The computational domain is $r \in [r_i / r_o, 1]$, $z \in [0, d/r_o]$ with $r = r_i / r_o + i(1 - r_i / r_o)/nr$ for $i \in [0, nr]$, and $z = j(d/r_o)(1 - r_i / r_o)/nz$ for $j \in [0, nz]$ (for the results presented here, $nr = nz = 160$, $d/r_o = 0.8$, and $r_i / r_o = 0.7865$).

Starting from a set of given initial conditions, the interior values of $\Gamma_{i,j}$ and $\eta_{i,j}$ ($i \in [1, nr-1]$ and $j \in [1, nz-1]$) are evolved forward in time using a second-order predictor-corrector scheme. Denoting the current time by superscript k, the predictor stage by superscript *, and the next (corrected) stage by $k + 1$, we first evaluate

$$\Gamma^*_{i,j} = \Gamma^k_{i,j} + \delta t \ \ RHS^k_1,$$

and

$$\eta^*_{i,j} = \eta^k_{i,j} + \delta t \ \ RHS^k_2 \ .$$

At this stage, we need to solve the elliptic equation (3) for ψ^* with the interior points for η^* just computed. Then, the surfactant concentration is advected by this streamfunction. So equation (6) is solved for c^* with ψ^*, and the boundary conditions $\partial c/\partial r = 0$ at $r = r_i/r_o$ and 1 (thus conserving total surfactant on the interface). This evolution is also done by the predictor-corrector scheme. One needs to do the full two stages to get from* c^k to c^{**} to c^* both stages using ψ^*. With $c^*(r)$, we evaluate $\sigma(c^*(r))$, $\lambda(c^*(r))$, $\kappa(c^*(r))$, and their radial derivatives. The boundary conditions for Γ^* and η^* are then evaluated. On the no-slip boundaries, this is straight forward. For the interface, we require the normal derivative of ψ at the interface (use one-sided differences) and its radial variations, and then solve equations (7, 8). Equation (7) is a second-order ODE for Γ at $z = d$, which reduces to a tridiagonal solve. Equation (8) is a straight forward evaluation now that we have the surface tension gradient and surface viscosities and their gradients. We now have everything (Γ, η, ψ, and c) at the predictor stage, and can repeat the whole process to everything to the corrector stage. We evolve Γ and η using

$$\Gamma^{k+1}_{i,j} = 0.5(\Gamma^k_{i,j} + \Gamma^*_{i,j} + \delta t \ \ RHS^*_1),$$

and

$$\eta^{k+1}_{i,j} = 0.5(\eta^k_{i,j} + \eta^*_{i,j} + \delta t \ \ RHS^*_2).$$

The explicit time stepping technique places a CFL-type restriction on the time step which is more severe as c_o and Pe^s increase. For the results presented here, δt was in the range 10^{-2} - 10^{-4}.

RESULTS

All the results presented here are in the annular deep-channel geometry for $Re = 2000$ and $Ca^{-1} = 3630$. For an air/water interface with a hemicyanine monolayer, there are only two parameters that have not been directly measured. These are the surface Peclet number, Pe^s, and the (non-dimensional) surface dilatational viscosity, κ, which varies with c. In the following, we shall present how this system behaves for various Pe^s with κ set equal to λ in the low c regime, where the elasticity in relatively low. In this flow regime, when the initial uniform surfactant distribution has $c_o < 0.35$, the bulk flow is able to overcome the elasticity of the interface and clean a portion of it, forming Reynolds ridge separating the clean from the contaminated surface (see Scott 1982).

Effects of Pe^s on the contamination front

Effects of Pe^s are only important when there are large gradients in c (this is particularly so at the contamination front). At the contamination front, the large jump in concentration leads to a large production of surface azimuthal vorticity, η at $z = d$, from the $\partial\sigma/\partial r = \partial\sigma/\partial c\ \partial c/\partial r$ term in (8). The surfactant front is distinguished by a sharp peak in η, whose width varies as $1/\sqrt{Pe^S}$. Figure 4 shows the effect of varying Pe^s on η at $z = d$ (in these calculations, the surface viscosity terms in (7) and (8) were artificially set to zero, since these terms will also have a tendency to smear out the contamination front). This plot indicates that for hemicyanine at $Re = 2000$, the corresponding surface diffusivity ($Pe^s > 10^6$) would not alter the surfactant distribution behind the contamination front. (We introduce a radial gap coordinate, $x = (r - r_i / r_o) / (1 - r_i / r_o)$).

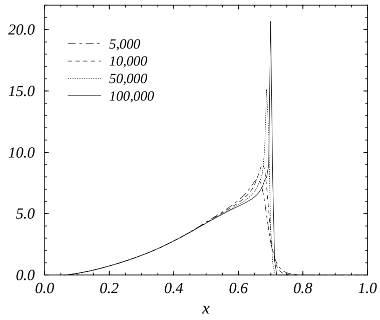

Figure 4: Azimuthal vorticity profiles, η at $z = d$, for various Pe^s as indicated, with $c_o = 0.25$ and zero surface viscosities.

The bulk secondary flow, which drives the interfacial flow, is depicted in Figure 5, showing the contours of the streamfunction ψ. This bulk flow overturns in the counter-clockwise direction.

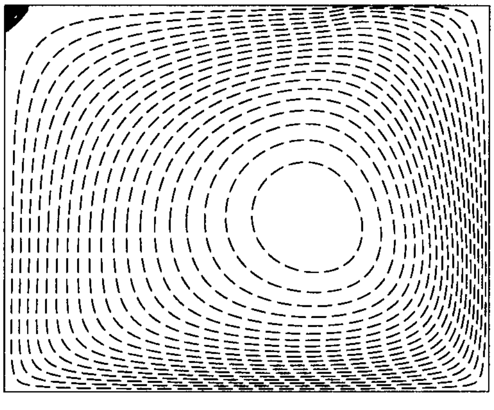

Figure 5: Streamfunction contours with $c_o = 0.25$.

Effects of c_o on the contamination front

A contamination front only forms when there is a balance between the interfacial viscoelasticity and the bulk flow near the interface. In the absence of the viscoelasticity, the surfactant molecules would act as passive scalar, advected by the bulk flow at the interface, and so would accumulate at the inner cylinder wall since they are insoluble. For a description of the flow in this geometry, in the absence of surfactants, see Lopez & Hirsa (1998).

There are three mechanisms at play that prevent such a build up at the inner cylinder wall, each of which dominate at different concentration and concentration gradient levels. If the concentration levels tend to become large (as they would be if the surfactants started to pile up at the inner cylinder), then their finite diffusivity, Pe^s, would oppose such a build up, smearing them out over a length $1/\sqrt{Pe^S}$. Such a mechanism would also be present if c were a passive scalar. However, c is an active scalar that determines the surface tension and surface viscosities (through equations 4 and 5), which in turn determine the stress balances at the interface that feed into the bulk flow as boundary conditions for the vorticity and angular momentum. This then introduces two additional mechanisms which resist the surfactant pile up and also tend to smear out any contamination front. The surface viscosities will tend to oppose the build up of surfactant by the bulk flow compression of the interface; this is triggered not only by the concentration gradient, but also by the concentration level. Figure 3 shows how λ increases exponentially with c for hemicyanine. The third mechanism, which in the cases presented here is dominant, is the Marangoni stress $\partial\sigma/\partial r$ which imparts an elasticity to the interface that resists the build up of surfactants due to the stretching and compacting of the interface by the bulk flow. For the insoluble system being studied, however, once the concentration level drops below a certain level (about $c = 0.3$), the Marangoni stress mechanism essentially vanishes (see Fig. 2), allowing the surface to be cleaned by bulk flow advection. As the concentration builds up at small radii, the Marangoni stress rapidly increases, and this mechanism tends to smear the surfactants out towards a uniform concentration. So we find that the contamination front essentially forms where the competition between the bulk flow advection and the Marangoni stress just balance, and this for our bounded, insoluble system depends critically on the total amount of surfactant residing on the interface. We measure this by c_o, the initial uniform concentration distribution.

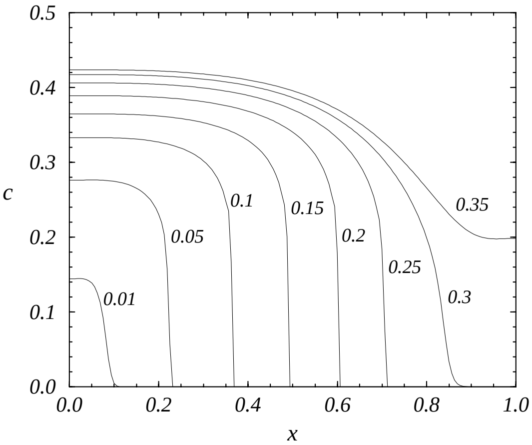

Figure 6: Surfactant concentration profiles c at steady state, with initial uniform distribution $c = c_o$, for c_o as indicated.

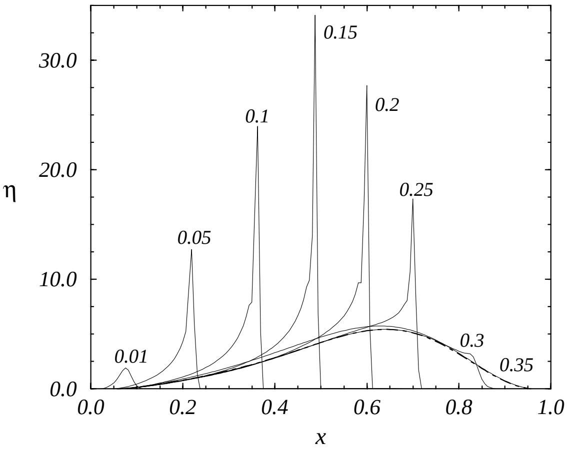

Figure 7: Azimuthal vorticity profiles, η *at* $z = d$, for various initial uniform distribution $c = c_o$, for c_o as indicated; the dot-dash line corresponds to a no-slip surface.

Figures 6 and 7 show the steady state concentration distributions and azimuthal vorticity profiles at the interface that result for different values of c_o. We find that if the initial concentration level is very low ($c_o < 0.01$), the Marangoni stress is essentially zero, the bulk flow advects all the surfactant in towards the inner cylinder, and the surface diffusion (and to a lesser extent the surface viscosity) mechanism determines the equilibrium surfactant distribution. For c_o between about 0.05 and 0.28, the Marangoni stress dominates in the determining the equilibrium c distribution, and the radial location of the contamination front varies linearly with c_o. For c_o above about 0.3, the Marangoni stress is so large that it completely dominates, not only the surface diffusion and viscosities, but also the bulk flow, and it almost completely resists the formation of surfactant gradients. These values of c_o are for the strength of the secondary bulk flow corresponding to $Re = 2000$ and $d/r_o = 0.8$. For larger Re and smaller d/r_o, the secondary flow is stronger and the c_o range over which a contamination front can form is extended.

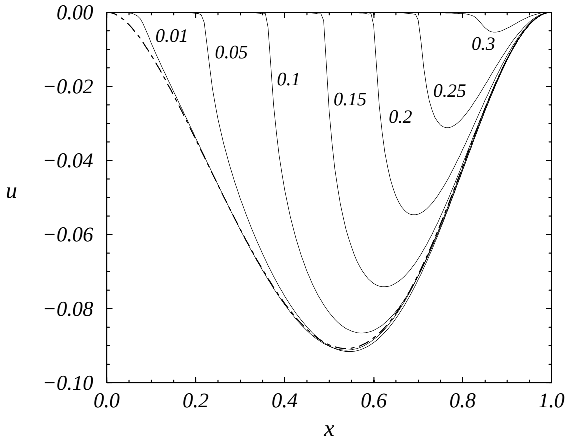

Figure 8: Radial velocity profiles, u at $z = d$, for various initial uniform distribution $c = c_o$, for c_o as indicated; the dot-dash line corresponds to a clean interface.

Typically when the Marangoni stress is dominating, the interface is thought of as immobile, acting as a no-slip surface. But this is only true for the velocity components in the directions that would have led to surfactant concentration. So in this axisymmetric swirling flow, this direction is radial. In the azimuthal direction, since the flow is axisymmetric, there are no azimuthal gradients of surfactant (or anything else for that matter), and so there are no Marangoni stresses acting in that direction. The result is that in the radial direction, the Marangoni stress makes the interface act like a no-slip surface, but in the azimuthal direction it is essentially stress-free (there are some contributions from the surface shear viscosity, through equation 7). Figures 8 and 9 illustrate this phenomena. This has fundamental consequences for models of contaminated interfaces that are not two-dimensional; surfactant coverage does not simply mean that the interface is no-slip.

It is of interest to compare our results with recent numerical models of contaminated gas/liquid interfaces. Bel Fdhila & Duineveld (1996) considered the steady rise of an air bubble in water where surfactants accumulated on the bubble surface for Reynolds numbers up to 500. They modeled the interface as being stress-free upstream, and no-slip downstream, of a contamination front. In the bubble dynamics literature, the contaminated downstream part is often called a stagnant cap. As is typical in bubble models, they impose the location of the front (aka the cap angle). Although they do not solve for the stress balance as would be described by equations of the form (7) and (8), they do obtain very similar results for η and u at the interface. Comparing their figure 4 with our figure 7, one sees very similar behavior; the sharp peak in η at the front, the strength of the peak reaching a maximum when the front forms at the half-way mark (mid-gap in our annulus and at the bubble equator), and how η approaches the profile corresponding to a no-slip solid wall downstream of the front. Their figure 6 and our figure 8 for the streamwise velocity at the interface also show a striking similarity. In both cases, the streamwise velocity asymptotes to that corresponding to a stress-free interface as the interface is cleaned (as is to be expected), and downstream of the contamination front, this velocity component goes to zero. In spite of this level of agreement, the straightout use of the no-slip condition on the contaminated side of the front is not appropriate; if it was, then *v* would vanish, yet when the proper stress-balance is imposed, *v* clearly does not vanish (see Fig. 9).

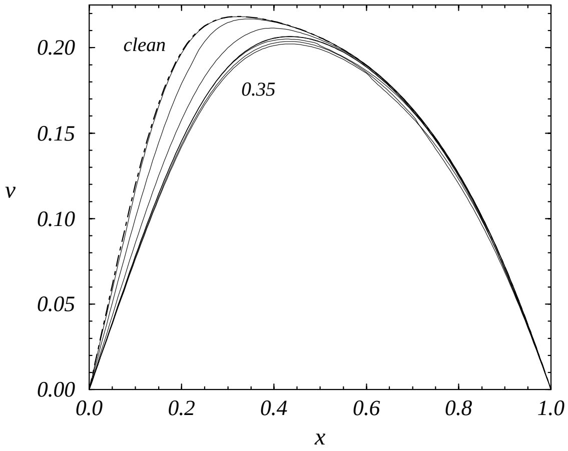

Figure 9: Azimuthal velocity profiles, *v* at $z = d$, for various initial uniform distribution $c = c_o$, for c_o as indicated in figure 7; the dot-dash line corresponds to a clean interface.

CONCLUSION

A fully coupled viscoelastic interfacial flow with a swirling bulk flow has been modeled numerically for flow and material properties corresponding to a physical air/water system with a hemicyanine monolayer. For the present numerical calculations, the equation of state, $\sigma(c)$, was measured in the laboratory for the hemicyanine modeled in this study. The calculations show that the surfactant distribution and the stress balance are critically dependent on the form of this function which can vary significantly between different classes of surfactants (namely gas-, liquid-, or solid-like surfactants systems; e.g. see Adamson, 1990; Gaines, 1966) as well as between different surfactants in a given class. There are additional factors that will play a role in determining the hydrodynamic coupling between the interface and the bulk if the surfactant has finite solubility in the bulk.

For the results presented here, in the small concentration regime, the Marangoni elasticity dominated, by several orders of magnitude, any surface viscosity effects. Work is underway to explore regimes where the elastic and viscous terms are more comparable, and in these viscoelastic regimes we hope to be able to estimate the surface dilatational viscosity.

ACKNOWLEDGEMENTS

We would like to thank Mr. C. M. Tomaso for conducting some of the experiments. This work was supported by NSF grants CTS-9803478 and CTS-9896259.

REFERENCES

ADAMSON, A. W., (1990) *Physical Chemistry of Surfaces*, (Wiley-Interscience Publication).

AGRAWAL, M. L. and NEUMAN, R. D., (1988) "Surface diffusion in monomolecular films. II. Experiment and theory," *J. Colloid Interface Sci.*, **121**, 366-380.

BEL FDHILA, R. and DUINEVELD, P. C., (1996) "The effect of surfactant on the rise of a spherical bubble at high Reynolds and Peclet numbers," *Phys. Fluids*, **8**, 310-321.

EDWARDS, D. A., BRENNER, H. and WASAN, D. T., (1991) *Interfacial Transport Processes and Rheology*, (Butterworth-Heinemann, Stoneham, MA).

GAINS, G. L., (1966) *Insoluble Monolayers at Liquid-Gas Interfaces*, (Interscience Publishers).

HIRSA, A., KORENOWSKI, G. M., LOGORY, L. M. and JUDD, C. J., (1997), "Determination of surface viscosities by surfactant concentration and velocity field measurements for an insoluble monolayer," *Langmuir*, **13**, 3813-3822.

LOPEZ, J. M. and CHEN, J., (1998), "Hydrodynamic coupling between a viscoelastic gas/liquid interface and a swirling vortex flow," *J. Fluids Eng.*, **120**, 655-661.

LOPEZ, J. M. and HIRSA, A., (1998), "Direct determination of the dependence of the surface shear and dilatational viscosities on the thermodynamic state of the interface: Theoretical foundations," *J. Colloid Interface Sci.*, **206**, 231-239.

SCOTT, J. C., (1982), "Flow beneath a stagnant film on water: the Reynolds ridge," *J. Fluid Mech.*, **116**, 283-296.

SCRIVEN, L. E., (1960), "Dynamics of a fluid interface," *Chem. Engng. Sci.* **12**, 98-108.